Finite Fracture Mechanics crack initiation from a circular hole

Finite Fracture Mechanics crack initiation from a circular hole

A. Sapora [a]*, A.R. Torabi[b], Siavash Etesam[b], P. Cornetti[a]

[a] *Department of Structural, Geotechnical and Building Engineering, Politecnico di Torino, 10129, Torino, Italy*

[b] *Fracture Research Laboratory, Faculty of New Sciences & Technologies, University of Tehran, P.O. Box 14395-1561, Tehran, Iran*

* Corresponding Author: alberto.sapora@polito.it

Abstract

The brittle crack initiation from a circular hole in an infinite slab under uniaxial remote tensile load is investigated. The analysis consists of two parts. The former is focused on the difference between symmetric and asymmetric crack propagation. Different criteria in the framework of Finite Fracture Mechanics (FFM) are implemented, and the potentiality of coupled stress and energy approaches is highlighted from a theoretical point of view. The latter presents the experimental results obtained by carrying out *ad-hoc* tensile tests on PMMA and GPPS notched samples, and the related FFM investigation.

KEYWORDS: Circular hole, brittle failure, symmetric propagation, FFM, tensile tests.

1. Introduction

Finite Fracture Mechanics (FFM) investigates brittle failure of cracked or notched structures by assuming that fracture propagates (at least at the first step) by a finite crack extension Δ. Different criteria have been proposed in this framework since the middle of the nineties, although the idea of a discretely propagating crack was put forward even before (Neuber 1953, Novozhilov 1969, Ritchie et al. 1973).

FFM approaches can be classified into three main categories: i) stress-based approaches (Taylor 1999, Seweryn 1994); ii) energy based approaches (Lazzarin and Zambardi 2001, Seweryn and Lukaszewicz 2002); iii) coupled stress and energy approaches (Leguillon 2002, Carpinteri et al. 2008). Criteria belonging to the first two groups involve a unique equation and the crack advance Δ

results to be a material constant, depending merely on the material tensile strength σ_u and on the fracture toughness K_{Ic}. On the other hand, coupled stress and energy based approaches are described by a system of two equations: the crack advance Δ becomes a structural parameter, and it represents one of the output of the FFM system, together with the failure load.

FFM approaches have been applied to different geometries, materials, and loading conditions. Some recent applications include, among the others, the failure behaviour of metals even under moderate or large scale yielding (Madrazo et al. 2012, Torabi and Alei 2016, Torabi et al. 2016a, Sapora and Firrao 2017), the investigation of three dimensional effects (Saboori et al. 2016, Yosibash and Mittelman 2016), the description of T-stress effects on the straight and curved crack deflection (Cornetti et al. 2014, Sapora et al. 2017), and the study of crack nucleation in negative geometries (Weißgraeber et al. 2016). From the comparison between theoretical predictions and experimental data it is generally difficult to determine which criterion predicts more accurately the failure initiation, changing the situation for each experimental test. From one point of view, the implementation of stress or energy criteria generally results more simple, since only one equation has to be solved. Furthermore, the stress field or the stress intensity factor (SIF, providing the crack driving force) functions can be derived easily, either analytically from the Literature or numerically from a simple Finite Element Analysis (FEA). From another point of view, these approaches present some drawbacks overcome by the coupled criteria (Carpinteri et al. 2008): they can be considered more physically sound, since both stress and energy requirements are satisfied, and their extension to more complex geometries (i.e., interfacial cracks, see (Munoz-Reja et al. 2016)) results straightforward. Finally, recent studies show that coupled approaches provide results very close to those by the cohesive zone model, once the constitutive law is properly defined (Henninger et al. 2007, Cornetti et al. 2016).
In the present work, a circular hole with radius R in an infinite plate under remote tensile load σ will be taken into account (Figure 1). Despite it represents one of oldest geometry analyzed in Fracture Mechanics, whose stress solution was obtained analytically by Kirsch more than one century ago, there remain some open questions from both the theoretical and the experimental points of view.

As concerns the first aspect, the novelty of the present work lies on the comparison between symmetric (Figure 1a) and asymmetric (Figure 1b) crack propagation. Although the difference is not high in terms of failure stress, the potentiality of coupled approaches will emerge once again, as already outlined by similar studies on different notched geometries (Garcia et al. 2015, Rosendahl et al. 2017).

As regards the experimental aspect, only few test results are available in the Literature (Li and Zhang 2006, Camanho et al. 2007). Furthermore, some of them present some drawbacks. Tensile tests on PMMA notched samples, for instance, were carried out by Li and Zhang (2006) and analyzed through different FFM criteria. The related FFM predictions were in rather poor agreement with experimental failure stresses, and it was concluded that only considering an additional material parameter (named as "material fracture toughness under tension") would lead to accurate predictions. The poorness of FFM results was observed also by Leguillon et al. (2007). On the other hand, in order to improve theoretical predictions, both the material properties of PMMA (i.e., σ_u and K_{Ic}) were fitted by Hebel et al. (2010): it was however concluded that the implemented values were "unrealistic" from a physical point of view. Maimi et al. (2013) performed a very accurate analysis, implementing also some cohesive zone models, mentioning but not implementing the data presented by Li and Zhang (2006).

Indeed, more comforting experimental results were carried out by Camanho et al. (2007) on Hexcel IM7-8552 carbon epoxy unidirectional laminates. In this case, the coupled FFM criterion was found to provide the most accurate predictions (Camanho et al. 2012).

According to the situation mentioned above, the second goal of the present paper is to provide a new set of experimental results for homogeneous polymeric materials by testing tensile PMMA and GPPS notched samples. Unfortunately, we were not able to verify the symmetric vs. asymmetric controversy with our testing instruments, but it will be shown that FFM predictions are in almost perfect agreement with experimental results, differently from those obtained by Li and Zhang (2006).

2. FFM approaches

Different FFM approaches are now briefly summarized. The notation will refer to the present geometry (Figure 1), for the sake of simplicity: thus, the notch tip will coincide with the point having coordinates $x=|R|$, $y=0$.

2.1 Stress based approaches

The most simple criterion is the point stress method (PM), according to which failure takes place when the stress σ_y at a finite distance Δ from the notch tip reaches the critical value σ_u. In formulae, we have:

$$\sigma_y(R+\Delta)=\sigma_u \tag{1}$$

with

$$\Delta=\frac{1}{2\pi}\left(\frac{K_{Ic}}{\sigma_u}\right)^2=\frac{1}{2\pi}l_{ch} \tag{2}$$

To the Author's best knowledge, the punctual stress idea dates back to Ritchie et al. (1973), where the elasto-plastic stress field was involved to take the failure micromechanics of metals into account and the well known RKR model was put forward. The criterion was later adapted to the linear elastic framework by Taylor (1999).

On the other hand, if the considered stress is averaged over Δ, the criterion is named line method (LM):

$$\frac{1}{\Delta}\int_R^{R+\Delta}\sigma_y(x)dx=\sigma_u \tag{3}$$

with

$$\Delta=\frac{2}{\pi}l_{ch} \tag{4}$$

The line method dates back to Neuber (1953) and Novozihlov (1969), and it was formalized for V-notches by Seweryn (1994).
Note that Eqs. (2) and (4) are not arbitrary: their expressions must be necessarily assumed to get $K_I=K_{Ic}$ (i.e, Linear Elastic Fracture Mechanics) for a cracked geometry.

2.2 Energy based approaches

According to the energy approach put forward by Seweryn and Lukaszewicz (2002), failure is achieved when the averaged energy available over a crack of length Δ reaches the fracture energy G_c:

$$\frac{1}{\Delta}\int_{R}^{R+\Delta} G(a)da = G_c \tag{5}$$

where a is the crack length and

$$\Delta = \frac{2}{\pi c^2} l_{ch} \tag{6}$$

The constant c is equal to 1 in case of a centre crack, and to 1.122 in case of an edge crack. Equation (6) must be necessarily implemented to get $\sigma=\sigma_u$ for a plain, un-notched geometry.

According to Irwin's relationship, it is possible to express Eq. (5) in terms of the SIF related to a crack of length a stemming from the notch tip $K_I(a)$ and the fracture toughness K_{Ic}, namely:

$$\frac{1}{\Delta}\int_{R}^{R+\Delta} K_I^2(a)da = K_{Ic}^2 \tag{7}$$

The approach described by Eq. (7) is also known as Quantized Fracture Toughness (QFM, Pugno and Ruoff 2004) .

Although not be implemented in this work, it is important to remind in this frameowrk the Strain Energy Density criterion (Lazzarin and Zambardi 2001), according to which the strain energy in a small volume surrounding the notch tip is responsible for crack initiation. The approach provides good results (e.g., Berto et al. 2013), but it generally requires a numerical implementation.

2.3 Coupled stress and energy approaches

Coupled approaches were proposed to overcome some drawbacks related to the criteria described above, especially as concerns size effects (Carpinteri et al. 2008). The coupled criteria can be expressed by coupling Eq. (7) either with Eq. (1) (Leguillon 2002)

$$\begin{cases} \sigma_y(\Delta + R) = \sigma_u \\ \dfrac{1}{\Delta}\displaystyle\int_{R}^{R+\Delta} K_I^2(a)da = K_{Ic}^2 \end{cases} \tag{8}$$

or with Eq. (3) (Carpinteri et al. 2008)

$$\begin{cases} \frac{1}{\Delta}\int_{R}^{R+\Delta} \sigma_y(x)dx = \sigma_u \\ \frac{1}{\Delta}\int_{R}^{R+\Delta} K_I^2(a)da = K_{Ic}^2 \end{cases} \quad (9)$$

From a mathematical point of view, both Eqs. (8) and (9) represent a system of two equations in two unknowns: the critical failure stress σ_f, implicitly embedded in the stress field and the SIF functions, and the crack advance Δ, which results to be a structural parameter, thus able to interact with the specimen size. Past studies on notched structures (Sapora et al. 2013, Campagnolo et al. 2016) showed that the former coupled criterion (Eq. (8)) provides higher failure loads and lower crack extensions than the latter approach (Eq. (9)). Furthermore, in case of mixed mode loading conditions, the crack propagation angle by Eq. (8) is generally a little higher.

From a physical point of view, coupled approaches state that fracture is energy driven, but a sufficiently high stress must act in order to trigger crack propagation. They are often simply referred to as FFM in the Literature. This nomenclature will be adopted hereafter.

3. Circular hole in an infinite plate under remote tensile load

In order to implement the FFM criteria described in the previous section, the stress field and/or the SIF functions are required.

For a circular hole in an infinite plate under remote tensile load σ (Figure 1), the stress field in the loading direction can be expressed as:

$$\sigma_y(x) = \frac{\sigma}{2}\left(2 + \frac{R^2}{x^2} + 3\frac{R^4}{x^4}\right) \quad (10)$$

providing the well-know stress concentration factor 3 for $x=R$. Far from the notch tip $x>>R$, the stress field keeps constant and equal the applied load σ.

On the other hand, the SIF function related to a crack of length a stemming from the notch root can be expressed as (Tada et al. 1985)

$$K_I(a) = \sigma\sqrt{\pi a}\, F(s) \quad (11)$$

with

$$s = \frac{a}{a+R} \tag{12}$$

The shape function F related to the symmetric crack propagation (Figure 1a)

$$F(s) = 0.5\ (3-s)\ [1+1.243(1-s)^3] \tag{13}$$

differs from that corresponding to the asymmetric crack case (Figure 1b):

$$F(s) = [1+0.2(1-s)+0.3(1-s)^6]\ F_1(s) \tag{14a}$$

with

$$F_1(s) = \left(2.243-2.64s+1.352s^2-0.248s^3\right) \tag{14b}$$

For a very large hole ($R>>a$, $s\rightarrow 0$) the notch-crack problem reverts to an edge crack subjected to the local peak stress, and F=1.122*3. On the other hand, for a vanishing radius ($R<<a$, $s\rightarrow 1$), we have that F=1 for the symmetric case and F=1/√2 for the asymmetric one.

The previous shape functions (Eqs. (11-14)) were obtained through a mapping function method by Tada et al. (1985), and the related accuracy was estimated to be better than 1%.

3.1 Symmetric vs. asymmetric crack propagation

Let us now compare some results by different FFM approaches starting from the case of a symmetric crack propagation (Figure 1). Predictions related to PM, QFM, and FFM (Eqs. (1), (7), and (8), respectively) are reported in Figure 2.

As can be seen, the limit $\sigma_f = \sigma_u / 3$ for very large radii is respected by all the criteria. On the other hand, for a vanishing root radius, QFM is not able to predict $\sigma_f = \sigma_u$. The inconsistency is related to the fact that c=1.12 is implemented in Eq. (6), overestimating the real failure load. The problem can

be overcome by setting c=1, but in this case the criterion fails to catch the other limit case, underestimating σ_f for large radii.

On the other hand, as regards the case of asymmetric crack propagation the curves are similar to the those depicted in Figure 2, with the following comments:

1) Predictions related to PM are exactly the same. As a matter of fact, the stress field does not vary and thus stress-based criteria (1) and (3) are not able to reveal any differences between symmetric and asymmetric crack propagation.

2) Predictions by the coupled criterion are a little higher than those corresponding to the symmetric case. Thus, from a theoretical point of view, the symmetric crack propagation has to be preferred. The situation is represented in Figure 3, where the curves related to the two different cases are plotted both by implementing both Eq. (8) and Eq. (9). Note that according to Eq. (9) the maximum percent deviation is nearly 5.3% (R/l_{ch} ~ 0.16) and it decrease as larger radii are considered. Differences related to Eq. (8) are even lower (nearly 3%). The FFM crack advance Δ is plotted in Figure 4, for both symmetric and asymmetric configurations. As stated before, in case of coupled criteria, the extension results to be a structural parameter, depending also on the radius R. The values for Δ lie between $4/\pi$ and $2/\pi$ $(1.12)^2$ ($R<<l_{ch}$ and $R>>l_{ch}$, respectively) for the asymmetric case, and between $2/\pi$ and $2/\pi$ $(1.12)^2$ for the symmetric case.

3) Predictions related to QFM are a little higher than those corresponding the symmetric case. Nevertheless, QFM presents another drawback, since for R=0 (but only in this case) the value $\Delta = 4/\pi l_{ch}$ should be implemented instead of Eq. (6) in order to achieve $\sigma_f = \sigma_u$. This is because, for a vanishing radius, the problem reverts to an infinite plate with a (virtual) centre crack of length a and not $2a$. Note that this inconvenient is overcome by the coupled criteria, where a regular transition for the crack advance between the extreme values is achieved (Figure 4).

Finally, it is important to point out that similar FFM studies were recently proposed. Garcia et al. (2015) solved the controversy about the symmetry of the debond onset at the fibre-matrix interface in single-fibre specimens under transverse tension. Through the coupled FFM criterion, it was predicted that an asymmetric (i.e. with a single debond) post-failure configuration refers to a lower critical remote tension than the symmetric one, the difference being above 10% in some cases. This result was imputable to the shielding effect between the two debonds in the symmetric solution,

confirming the experimental evidences found in the literature. On the other hand, the analysis performed by Rosendahl et al. (2017) was more sophisticated than the present one, considering a combined tensile and in-plane bending loading. It was found that the bending contribution plays a crucial role in determining whether the crack configuration results to be symmetric or asymmetric.

4. Experimental investigation

Two series of tensile tests were carried out on notched structures made of PMMA and GPPS, respectively. Notched specimens were obtained from a PMMA sheet with the following dimensions (Figure 5): l = 100mm, w = 40 mm, and t = 10 mm. The GPPS sample dimensions were exactly the same, except for t = 8 mm. In both cases, the thickness was large enough to get plane strain conditions. Four different geometries were considered for each material, machining a circular hole with diameter $2R$=0.5, 1, 2, 4 mm. With the present assumption ($w/2R > 10$), the hypothesis of an infinite plate is reasonable and the formulae presented in Section 3 can be applied without loss of accuracy.

Three different specimens were considered for each geometry, both for PMMA and GGPS, for a total of 24 tensile tests. Critical values of the load under which crack starts to propagate from the notch tip, recorded on the tensile testing machine, are provided in Table 1.

The experimental fracture was of brittle character and no plastic strains were observed during tests: the force-displacement curves recorded for $2R$=0.5 mm (PMMA, test 1) and for $2R$=4 mm (GPPS, test 1) during failure are reported in Figures 6 and 7, respectively, along with related tested specimens.

The material properties had been already evaluated experimentally by one of the Author in some previous works (Ayatollahi and Torabi 2010,Torabi et al. 2016b), following the procedure described in ASTM standard codes. According to the values reported in Table 1, $l_{ch} = 0.773\,\text{mm}$ for PMMA (thus R/l_{ch} lies between 0.32 and 2.6), and $l_{ch} = 2.18\,\text{mm}$ for GPPS (thus R/l_{ch} lies between 0.12 and 0.92). The whole R/l_{ch} range of practical interest was thus covered (Figure 3).

4.1 FFM results

Unfortunately, it was not possible to distinguish precisely between symmetric and asymmetric crack initiation with our instruments, since a sophisticated recording camera would be needed. The crack propagation appeared to be symmetric at naked eye. On the other hand, from a practical point of

view, an asymmetric propagation would have probably to be preferred (especially for large radii, see Figure 3) due to the influence of micro-defects which generally affect the material behaviour.
In any case, due to the small difference between the two types of propagation in terms of failure load and coherently to what already presented in the Literature (Leguillon et al. 2007, Hebel et al. 2010, Camanho et al. 2012), symmetric FFM results were implemented. For PMMA, they are reported in Figure 8 together with experimental data. According to both coupled approaches (Eq.(8) and Eq.(9)), the maximum percentage error with respect to the experimental average failure stress does not exceed 10%, which can be considered more than satisfactory. Indeed, the value of σ_u to be used could be not that obtained by testing plain specimens, since their failure behaviour is affected by the presence of micro-cracks/defects or crazing phenomena (Taylor 2007). As a matter of fact, the real σ_u can be larger than the experimental value and its value has to be fitted (often the parameter is re-termed as σ_0) according to theoretical predictions. FFM results (Eq.(9)) by implementing a tensile strength corresponding to σ_u = 82.5 MPa are reported in Figure 8: the maximum percentage error decreases to 5%.
Analogous considerations hold for GPPS tested samples. FFM results and experimental failure stresses are reported in Figure 9. Predictions are again satisfactory. Indeed, those related to Eq. (9) seem to be generally more precise, the maximum percentage error with respect to the experimental average failure stress being nearly 7% ($2R$=0.5 mm). It decreases to less than 5% by implementing a fitted tensile strength value, namely σ_u = 31.5 MPa.

Finally, some comments should be added on the similar experiments carried out by Li and Zhang (2006): the sample geometry was similar (actually w=30 mm instead of 40 mm), and the material was PMMA (K_{Ic} = 1.00 MPa $\sqrt{m}$, σ_u = 72 MPa). Four different radii were machined, corresponding to $2R$= 0.6, 1.2, 2 and 6 mm. On the other hand, FFM predictions underestimate the experimental data by more than 30%, except for the largest radius hole size, where it decreases to 15%. A possible explanation, looking also at the apparent nonlinear stress-displacement curves shown in the paper, could be related to some nonlinear/ductile mechanisms which took place and influenced significantly the recorded results, as suggested also by Hebel et al. (2010).

5. Conclusions

The crack initiation from a circular hole in an infinite plated under uniaxial tension was investigated through different FFM approaches, by comparing symmetric and asymmetric crack propagation.
From a theoretical point of view, stress based criteria are not able to reveal any differences, but coupled criteria predict that a symmetric crack propagation has always to be preferred, since it leads

to a lower failure load. Similar results are provided by energy approaches such as QFM, which however is not able to provide, at the same time, the correct results for the limit cases of vanishing and large holes.

PMMA sand GPPS samples containing holes with different radii, sufficiently small with respect to the specimen width in order to reproduce an infinite geometry, were tensile tested. If, from one point of view, we were not able to realize with precision if crack propagation was symmetric or not, from another point of view, size effects were well caught by FFM. These data thus form a new reliable set of experimental results in the Literature for what concerns homogeneous polymeric materials containing a circular hole.

References

Ayatollahi, M.R., Torabi, A.R. (2010). Investigation of mixed mode brittle fracture in rounded-tip V-notched components, *Engineering Fracture Mechanics* 77, 3087–3104.

Berto, F., Campagnolo, A., Elices, M., Lazzarin, P. (2013). A synthesis of Polymethylmethacrylate data from U-notched specimens and V-notches with end holes by means of local energy. *Materials & Design* 49, 826-833.

Berto, F., Lazzarin, P. (2014). Recent developments in brittle and quasi-brittle failure assessment of engineering materials by means of local approaches, *Materials Science and Engineering R* 75, 1–48.

Camanho, P.P., Maimí, P., Dávila, C.G. (2007). Prediction of size effects in notched laminates using continuum damage mechanics. *Compos Sci Technol* 67, 2715–27.

Camanho, P.P., Erçin, G., Catalanotti, G., Mahdi, D., Linde, P. (2012). A finite fracture mechanics model for the prediction of the open-hole strength of composite laminates, *Composites Part A: Applied Science and Manufacturin*g 43, 1219–1225.

Campagnolo, A., Berto, F. , Leguillon, D. (2016). Fracture assessment of sharp V-notched components under Mode II loading: a comparison among some recent criteria. *Theoretical and Applied Fracture Mechanics* 85, 217–226.

Carpinteri, A., Cornetti, P., Pugno, N., Sapora, A., Taylor, D. (2008). A finite fracture mechanics approach to structures with sharp V-notches, *Engineering Fracture Mechanics* 75, 1736–1752.

Cornetti, P., Sapora, A., Carpinteri, A. (2014). T-stress effects on crack kinking in Finite Fracture Mechanics. *Engineering Fracture Mechanics* 132, 169-176.

Cornetti, P., Sapora, A., Carpinteri, A. (2016). Short cracks and V-notches: Finite Fracture Mechanics vs. Cohesive Crack Model, *Engineering Fracture Mechanics* 168, 2-12.

García, I.G., Mantič, V., Graciani, E. (2015). Debonding at the fibre–matrix interface under remote transverse tension. One debond or two symmetric debonds? *European Journal of Mechanics - A/Solids* 53, 75-88.

Hebel, J., Dieringer, R., Becker, W. (2010). Modelling brittle crack formation at geometrical and material discontinuities using a finite fracture mechanics approach, *Engineering Fracture Mechanics* 77, 3558‑3572.

Henninger, C., Leguillon, D., Martin, E. (2007). Crack initiation at a V-notch—comparison between a brittle fracture criterion and the Dugdale cohesive model. *Comptes Rendus Mécanique*, 335, 388-393.

Lazzarin, P., Zambardi, R. (2001). A finite-volume-energy based approach to predict the static and fatigue behavior of components with sharp v-shaped notches, *International Journal of Fracture* 112, 275–298.

Leguillon, D. (2002). Strength or toughness? A criterion for crack onset at a notch, *European Journal of Mechanics A/Solids* 21, 61–72.

Leguillon, D., Quesada, D., Putot C., Martin, E. (2007). Prediction of crack initiation at blunt notches and cavities – size effects. *Engineering Fracture Mechanics* 74, 2420–2436.

Li, J., Zhang, X. (2006). A criterion study for non-singular stress concentrations in brittle or quasi-brittle materials, *Engineering Fracture Mechanics* 73, 505–523.

Madrazo, V., Cicero, S., Carrascal, I.A. (2012). On the Point Method and the Line Method notch effect predictions in Al7075-T651, *Engineering Fracture Mechanics* 79, 363-379.

Maimí, P., González E.V., Gascons, N., Ripoll, L. (2013). Size effect law and critical distance theories to predict the nominal strength of quasibrittle structures. *Appl. Mech. Rev* 65, 020803.

Muñoz-Reja, M., Távara, L., Mantič, V., Cornetti, P. (2016). Crack onset and propagation at fibre–matrix elastic interfaces under biaxial loading using finite fracture mechanics, *Composites Part A: Applied Science and Manufacturing* 82, 267-278.

Neuber, H. (1958). Theory of notch stresses. Berlin: Springer.

Novozhilov, V. (1969). On a necessary and sufficient condition for brittle strength. *Prik Mat Mek* 33, 212–22.

Pugno, N., Ruoff, N. (2004). Quantized fracture mechanics, *Philosophical Magazine A* 84, 2829–45.

Ritchie, R.O., Knott, J.F., Rice J.F. (1973). On the relation between critical tensile stress and fracture toughness in mild steel, *J Mech Phys Solids* 21, 395–410.

Rosendahl, P.L., Weißgraeber, P., Stein, N., Becker, W. (2017). Asymmetric crack onset at open-holes under tensile and in-plane bending loading. *International Journal of Solids and Structures*, 113–114, 10-23.

Saboori, B. Ayatollahi, M.R., Torabi, A.R., Berto, F. (2016). Mixed mode I/III brittle fracture in round-tip V-notches, *Theoretical and Applied Fracture Mechanics* 83, 135-151.

Sapora, A., Cornetti, P., Carpinteri, A. (2013). A finite fracture mechanics approach to V-notched elements subjected to mixed-mode loading, *Engineering Fracture Mechanics* 97, 216–226.

Sapora, A., Cornetti, P., Mantic, V. (2016). T-stress effects on crack deflection: Straight vs. curved crack advance, *European Journal of Mechanics A/Solids* 60, 52-57.

Sapora, A. Firrao, D. (2017). Finite fracture mechanics predictions on the apparent fracture toughness of as-quenched Charpy V-type AISI 4340 steel specimens. *Fatigue & Fracture Of Engineering Materials & Structures* 40, 949-958.

Seweryn, A. (1994). Brittle fracture criterion for structures with sharp notches, *Engineering Fracture Mechanics* 47, 673–81.

Seweryn, A., Lukaszewicz, A. (2002). Verification of brittle fracture criteria for elements with V-shaped notches, *Engineering Fracture Mechanics* 69, 1487–1510.

Tada, H., Paris, P., Irwin, G. (1985). The stress analysis of cracks. Handbook. second ed., Paris Productions Incorporated, St Louis, MO, USA**.**

Taylor, D. (1999). Geometrical effects in fatigue: a unifying theoretical model, *International Journal of Fatigue* 21, 413–20.

Taylor, D. (2007) The Theory of Critical Distances: a New Perspective in Fracture Mechanics, Elsevier: Oxford, UK.

Torabi, A.R., Alaei, M. (2016). Application of the equivalent material concept to ductile failure prediction of blunt V-notches encountering moderate-scale yielding. *International Journal of Damage Mechanics* 25, 853–877.

Torabi, A.R., Campagnolo, A., Berto, F. (2016a). Mixed mode I/II crack initiation from U-notches in Al 7075-T6 thin plates by large-scale yielding regime. *Theoretical and Applied Fracture Mechanics* 86, 284-291.

Torabi, A.R., Majidi, H.R., Ayatollahi, M.R. (2016b). Brittle failure of key-hole notches under mixed mode I/II loading with negative mode I contributions, *Engineering Fracture Mechanics* 168, 51-72.

Weißgraeber, P., Hell , S., Becker, W. (2016). Crack nucleation in negative geometries. *Engineering Fracture Mechanics* 168, 93-104.

Yosibash, Z., Mittelman, B. (2016). A 3-D failure initiation criterion from a sharp V-notch edge in elastic brittle structures. *European Journal of Mechanics - A/Solids* 60, 70-94.

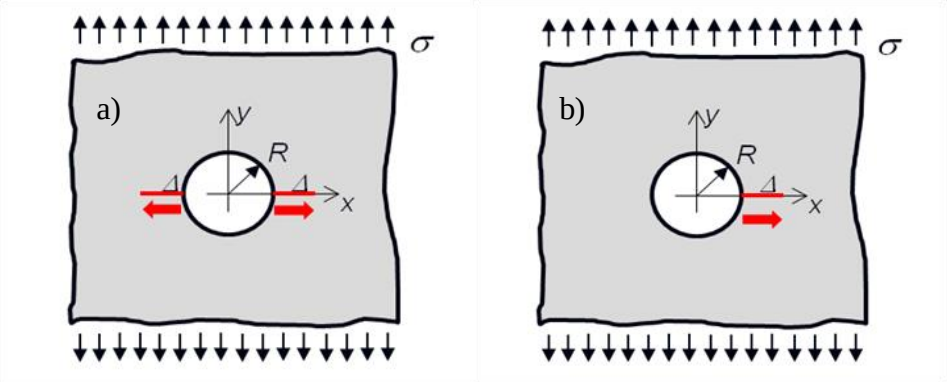

Figure 1. Circular hole in an infinite plate under remote tensile load σ: symmetric (a) vs. asymmetric (b) crack propagation.

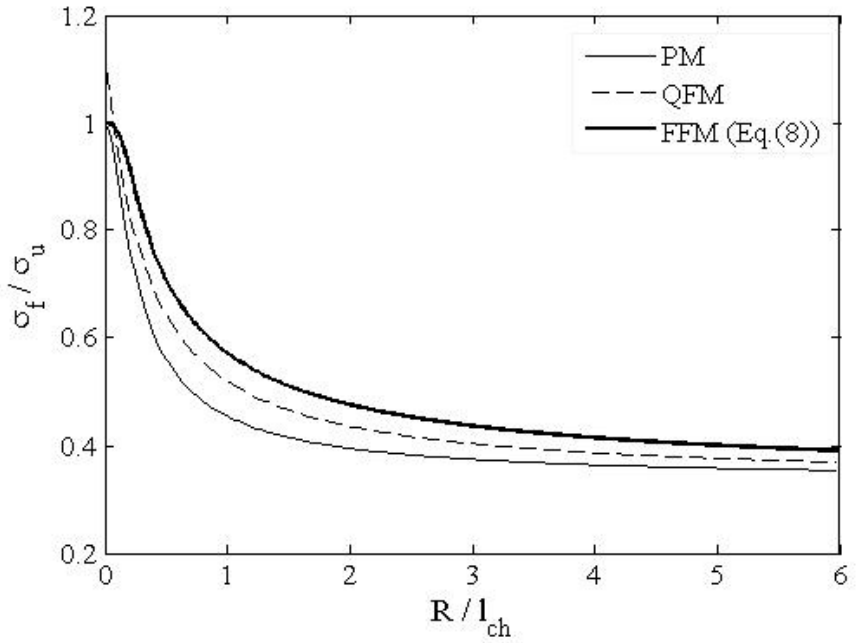

Figure 2. Symmetric crack propagation: dimensionless predictions according to different theoretical models.

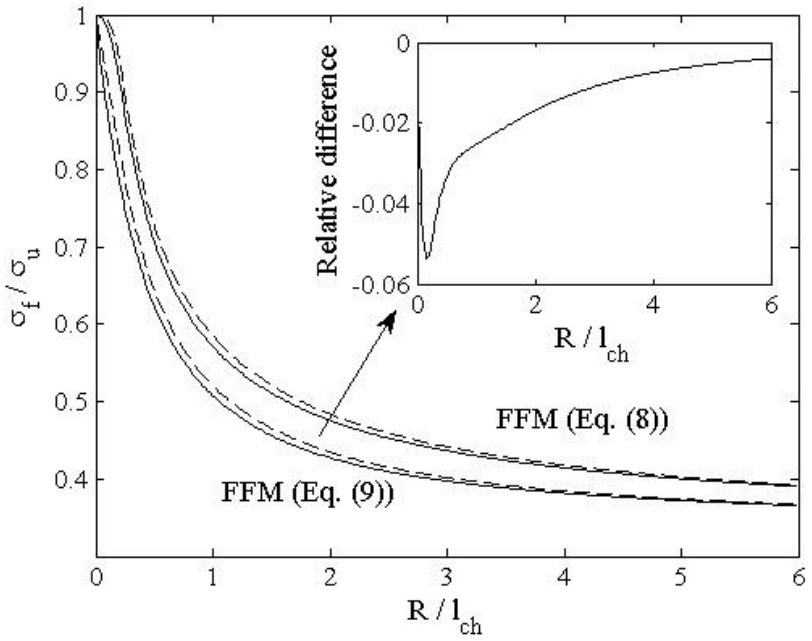

Figure 3. FFM dimensionless failure stress related to symmetric (continuous line) and asymmetric (dashed line) crack propagation according to both Eq. (8) (Leguillon 2002) and Eq. (9) (Carpinteri et al. 2008). The relative difference between predictions related to Eq. (9) is represented in the upper-right box.

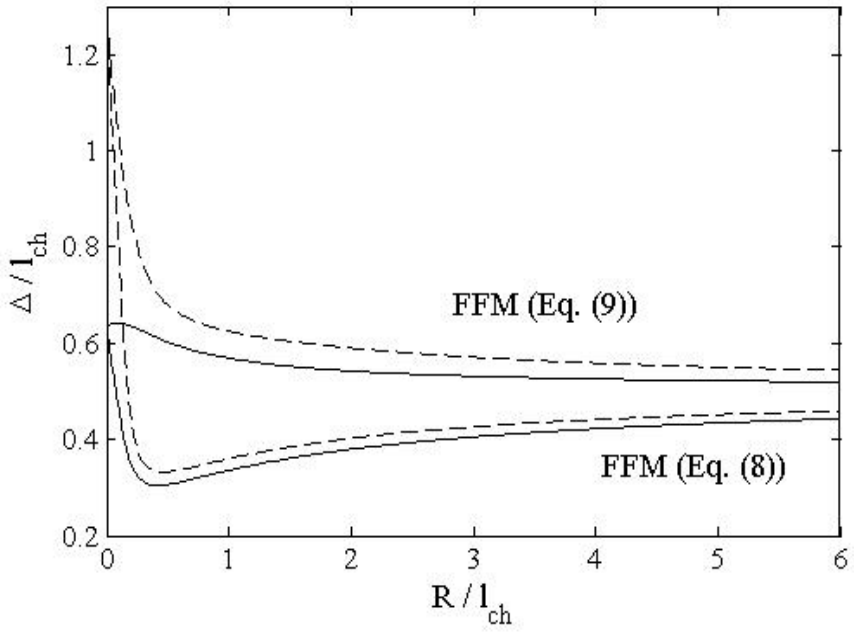

Figure 4. FFM dimensionless crack advance related to symmetric (continuous line) and asymmetric (dashed line) crack propagation according to both Eq. (8) (Leguillon 2002) and Eq. (9) (Carpinteri et al. 2008).

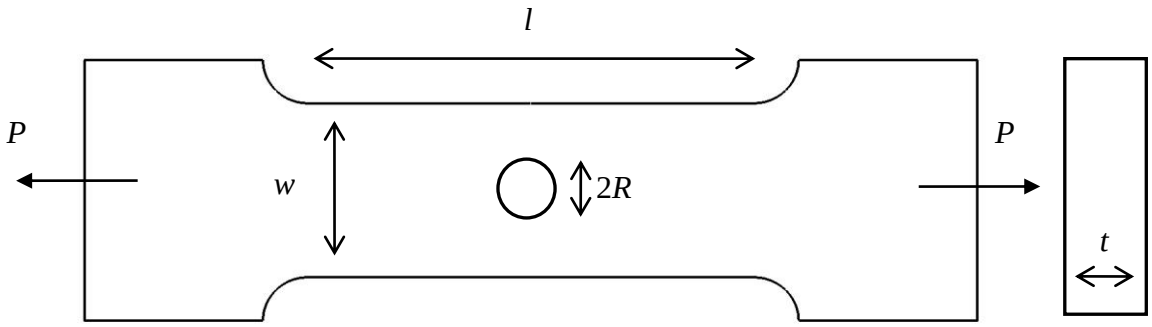

Figure 5. Geometry for the tensile notched sample.

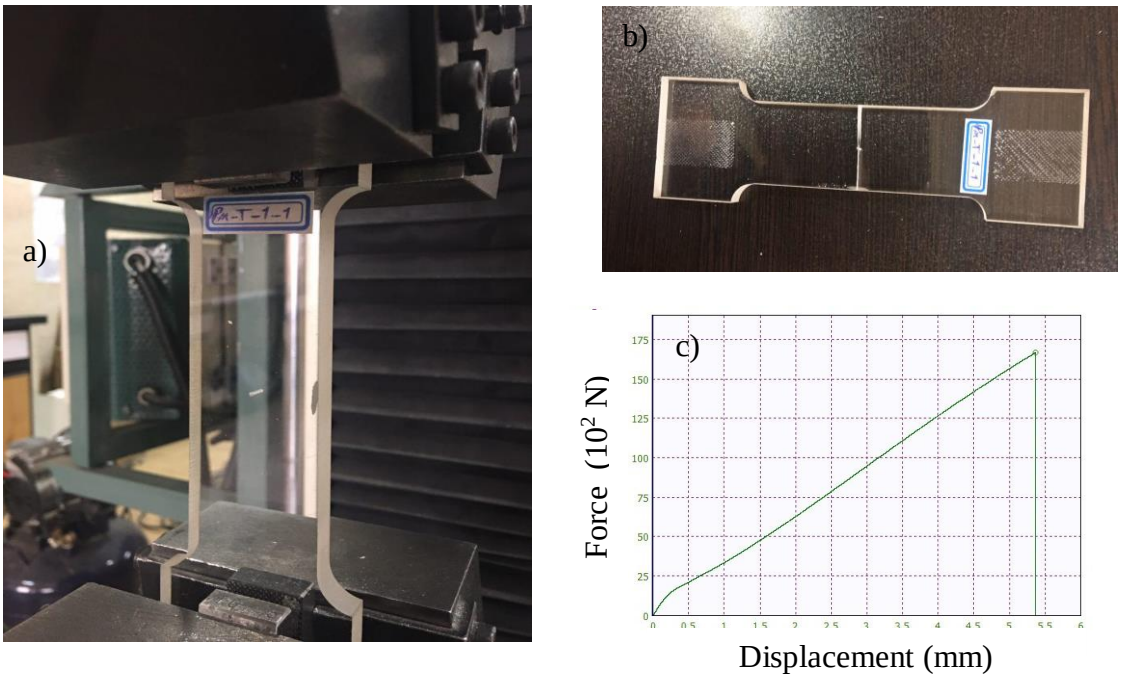

Figure 6. PMMA notched samples (2*R*=1mm, test 1): tensile test (a), broken specimen (b), recorded force-displacement curve (c).

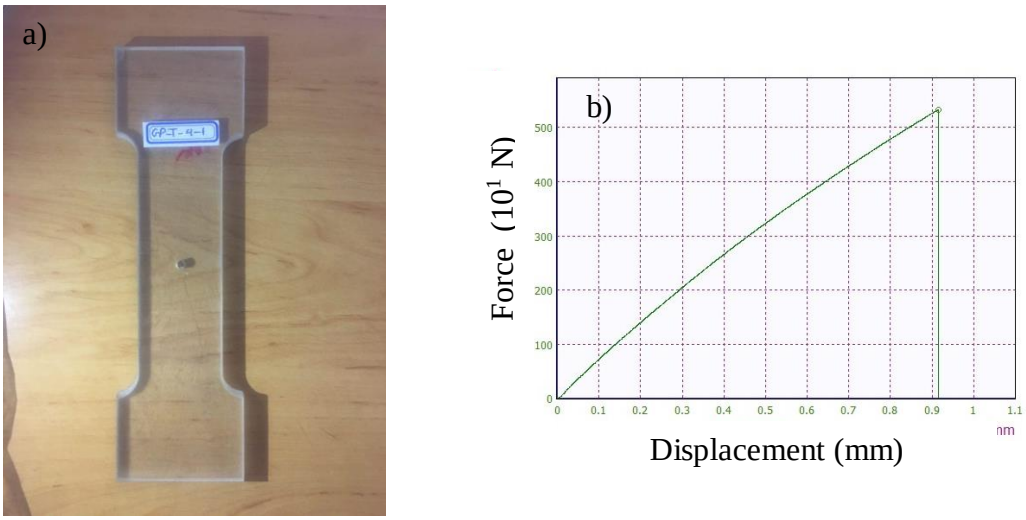

Figure 7. GPPS notched samples (2*R*=4mm, test 1): specimen before testing (a), recorded force-displacement curve during failure (b).

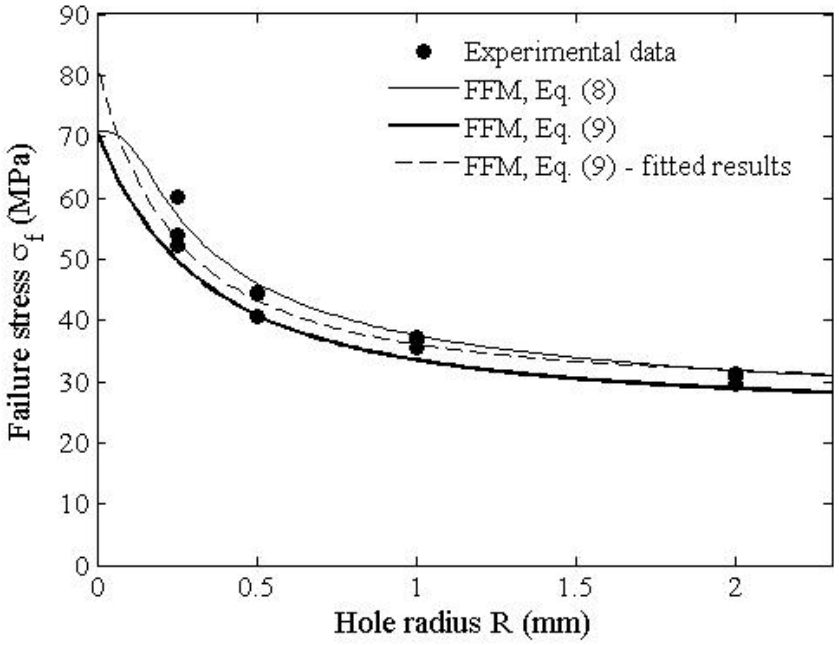

Figure 8. Tensile tests on PMMA notched samples: experimental failure stresses vs. FFM predictions.

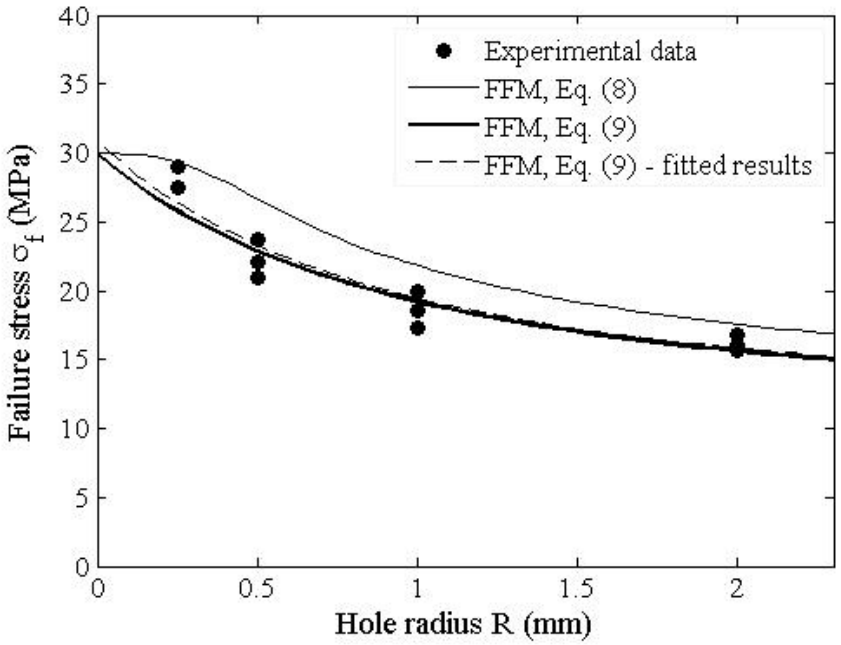

Figure 9. Tensile tests on GPPS notched samples: experimental failure stresses vs. FFM predictions

2R (mm) – Test index	PMMA K_{Ic} = 1.96 MPa √m, σ_u = 70.5 MPa		GPPS K_{Ic} = 1.40 MPa √m, σ_u = 30 MPa	
	P_{cr} (kN)	Average value (kN)	P_{cr} (kN)	Average value (kN)
0.5-1	24.100	22.200	9.050	8.730
0.5-2	21.600		8.580	
0.5-3	20.900		8.560	
1-1	17.800	17.250	7.400	6.950
1-2	17.700		6.900	
1-3	16.250		6.550	
2-1	14.900	14.600	6.210	5.800
2-2	14.650		5.780	
2-3	14.250		5.410	
4-1	11.800	12.200	5.250	5.050
4-2	12.250		4.900	
4-3	12.550		5.000	

Table 1. Experimental results: critical failure load P_{cr} (kN) for PMMA and GPPS specimens with different hole sizes. The material properties evaluated in (Ayatollahi and Torabi 2010,Torabi et al. 2016b) are also reported.